Collisional Energy Transfer in Unimolecular Reactions: Direct Classical Trajectories for $CH_4 \rightleftarrows CH_3 + H$ in Helium

Ahren W. Jasper* and James A. Miller*

Combustion Research Facility, Sandia National Laboratories, P.O. Box 969, Livermore, California 94551-0969

Received: January 27, 2009; Revised Manuscript Received: March 24, 2009

Direct classical trajectories are used to compute energy transfer parameters appropriate for use in master equation calculations for the $CH_4 \rightleftarrows CH_3 + H$ reaction in He at 300−2000 K. The quantum chemistry method used in the direct trajectory calculations is MP2/aug′-cc-pVDZ, which is validated against higher level ab initio calculations. The average energy transferred in deactivating collisions is shown to increase with the initial rotational excitation J' of CH_4 and with the temperature of the bath gas T_{bath}. When thermally averaged over J', the resulting average downward energy transfer α is found to increase nearly linearly with T_{bath} ($\alpha = 110 T_{bath}^{0.81}$ cm^{-1}). The results of master equation calculations carried out using the single-exponential-down model and the computed values of α are compared with experimental results and recent recommendations. At elevated temperatures (>600 K), good agreement between the predicted and experimental rate coefficients is obtained. At room temperature, the computed rate coefficients are in good agreement with the experimental results if the two-dimensional (E, J) formulation of the master equation is used. Smaller values of α (by 25%) are necessary to fit the experimental data at room temperature using the one-dimensional (E) master equation. The present study, combined with previous ab initio transition state theory calculations for the $CH_3 + H$ capture rate, provides a complete first-principles characterization of the temperature and pressure dependent rate coefficients for this simple single-well system.

I. Introduction

Master equation (ME) calculations[1−3] may be used to obtain temperature and pressure dependent rate coefficients for processes with complex potential energy surfaces, multiple intermediates, and competing products. The accuracy of these calculations depends on the accuracy of the underlying thermochemistry and elementary dynamics, as well as the treatment of collisional energy transfer. For small- and moderate-sized systems, well-validated quantum chemistry methods can be used to compute barrier heights and channel energies with so-called "chemical" accuracy (∼1−2 kcal/mol). Quantitative kinetics for elementary processes (e.g., bimolecular capture reactions, isomerizations, etc.) can be obtained using transition state theory, so long as suitable corrections are made to account for tunneling, barrierless transition states, vibrational anharmonicities, etc.

For many systems, the dominant source of error in the ME calculations is the treatment of collisional energy transfer, which accounts for the activation and stabilization of the intermediate complexes. In practice, one often empirically adjusts energy transfer parameters in the ME calculations to fit experimental data. These data are not always available, especially at pressures away from the high-pressure limit where the results of the ME are most sensitive to the treatment of collisional energy transfer. Furthermore, even when suitable experimental data are available, the transferability of the empirically derived energy transfer parameters to other conditions or to other systems is uncertain.

Since the early work of Stace and Murrell,[4] numerous studies[5−19] of collisional energy transfer between polyatomic target systems and monatomic bath gases have been carried out using classical trajectories. Although the details of the trajectory studies vary and few systematic studies exist, some general trends have emerged. Many studies have noted significant numbers of so-called "supercollisions", i.e., collisions transferring energies several times greater than the average energy transferred, and the energy transfer probability distribution has been observed to have a long tail that is not well-represented by a single exponential. Energy transfer typically increases linearly with the total energy of the target, although some studies suggest a more complicated energy dependence. Both increasing the initial rotational excitation of the target species and heating the bath gas have been show to enhance energy transfer. Details of the intermolecular bath-target potential energy surface have been shown to have some effect on energy transfer, whereas energy transfer is relatively insensitive to details of the intramolecular potential energy surface describing the internal structure of the target species.

In previous trajectory studies, empirical or fitted analytic many-body functional forms were typically used to describe the intramolecular potential energy surface of the target species, and pairwise additive functional forms (Lennard-Jones, "exp-6", etc.) were used to describe the interaction of the atomic bath gas and the target species. One exception is the work of Brunsvold et al.,[18] where an MSINDO semiempirical potential energy surface was used to describe ethane, and analytic pairwise additive forms were used for the interaction with the bath gas.

Here we use direct molecular dynamics (classical trajectories) to study collisional energy transfer for the CH_4 + He system and to determine energy transfer parameters for use in ME calculations of the $CH_4 \rightleftarrows CH_3 + H$ reaction. This work differs from much of the earlier work in two important ways. First, a full-dimensional, fully anharmonic potential energy surface is used to describe the CH_4 fragment *and* the CH_4−bath gas

* Address correspondence to either author. E-mails: ajasper@sandia.gov (Jasper), jamiller@sandia.gov (Miller).

10.1021/jp900802f CCC: $40.75
Published on Web 04/17/2009

interaction. Second, we compute highly averaged energy transfer parameters suitable for use in ME calculations directly, without attempting to resolve the underlying dynamical details.

There has been some previous theoretical work studying energy transfer in the $CH_4 \rightleftarrows CH_3 + H$ system. Hu and Hase[7] used classical trajectories to model energy transfer in Ar at 1000 K using three analytic potentials. Energy transfer parameters have also been obtained by fitting the results of ME calculations[20−22] to experimentally measured rates;[20,23−25] the energy transfer parameters obtained in these studies are dependent on various details of the ME calculations and may also be sensitive to the experimental data used.

The major goal of this research is the description and validation of a general and efficient strategy for obtaining energy transfer parameters directly for use in ME analyses of unimolecular reactions. This strategy, combined with ab initio transition state theory and quantum chemistry calculations, allows for a complete first-principles description of the kinetics of simple single-well systems.

II. Theory

A. Master Equation Analysis. The ME formalism employed here has been discussed in detail elsewhere.[3,21] Briefly, the two-dimensional ME for a simple irreversible dissociation reaction can be written

$$-k(T,P)x(E,J) = Z\sum_J \int_0^\infty P(E,J;E',J')x(E',J')\,\mathrm{d}E' - Zx(E,J) - k(E,J)x(E,J) \quad (1)$$

where $k(T, P)$ is the dissociation rate coefficient, $x(E, J)$ is the normalized population of CH_4 for each total energy E and total angular momentum J, Z is the collision rate and is assumed to be independent of E and J, $P(E, J; E', J')$ is the collisional energy transfer function, and $k(E, J)$ is the microcanonical rate coefficient.

The collisional energy transfer function describes the probability of a collision with the bath gas transferring the system from an initial state E', J' to some other state E, J. To simplify the solution of eq 1, this function can be written as

$$P(E,J;E',J') = P(E;E')\varphi(E,J) \quad (2)$$

where it is assumed that the rotational distribution after the collision is independent of E' and J'. This assumption allows eq 1 to be reduced to an equivalent one-dimensional ME that can be solved in a straightforward fashion.[21] Miller and co-workers[3,21] introduced the approximation

$$\varphi(E,J) = (2J+1)\rho(E,J)/\rho(E) \quad (3)$$

where $\rho(E, J)$ is the vibrational−rotational density of states at E and J and

$$\rho(E) = \sum_J (2J+1)\rho(E,J) \quad (4)$$

This approximation has the desirable property that $P(E, J; E', J')$ automatically satisfies detailed balance if $P(E; E')$ is constructed to do so. Equation 3 implies that the postcollision J distribution contains populations that are simply proportional to the number of states in the vicinity of any E and J. Although some subtle effects[3] are missing from this model, it includes all the effects on unimolecular rate coefficients normally associated with molecular rotation.

We adopt the exponential-down model

$$P(E,E') = \frac{1}{C_N(E')}\exp(-\Delta E/\alpha), \quad E \le E' \quad (5)$$

in our analysis. This model assumes that collisional energy transfer depends on $\Delta E = |E - E'|$ but not on E or E' independently. In the master equation calculations, collisions occurring with energies close to the threshold for dissociation are most important in determining the thermal rate coefficients. Collisional energy transfer has its largest effect on the unimolecular rate coefficient at the low-pressure limit. Under these conditions, except for states near the dissociation threshold, all the bound states have their equilibrium populations, and the unbound states have zero population (by definition of the limit). As the pressure increases, this picture changes in that the populations of unbound states begin to have nonzero populations, but at the same time collisional energy transfer has a smaller effect on the rate coefficient. At the high-pressure limit the rate coefficient is totally independent of collisional energy transfer. As a consequence of these properties, a simple model for energy transfer in which only the properties of bound states near the dissociation limit (E_{diss}) are taken into account is quite satisfactory. In eq 5, if $E_{diss} \gg \alpha$, α can be interpreted as the average energy transferred in a deactivating collision, $\langle \Delta E_d \rangle$.

Miller et al.[21] have shown that rate coefficients from ME analyses are relatively independent of the form used for $P(E, E')$ (for a specified $\langle \Delta E_d \rangle$) in methane dissociation. This result was not unexpected, and it is probably reasonable to conclude that such will be the case for any single-channel thermal dissociation. However, product distributions in multiple-channel dissociations and in chemically activated problems that involve low-lying (or high-lying) exit channels (isomerization or dissociation) are likely to depend critically on the form of $P(E, E')$, particularly on the existence or nonexistence of a long tail ("supercollisions"). In fact, Miller and Chandler[26] found large effects from such a tail in studying the overtone isomerization of methyl isocyanide. Such photoactivated problems are very similar energetically to chemically activated ones.

One can cast the integrals in the master equation in discrete form and write the ME as

$$\frac{\mathrm{d}|\mathbf{x}\rangle}{\mathrm{d}t} = \mathbf{M}|\mathbf{x}\rangle \quad (6)$$

where $|\mathbf{x}\rangle$ is the population vector and $\mathbf{M}$ is the transition matrix. Chemical reaction is associated only with the slowest relaxing eigenmode of $\mathbf{M}$, and the dissociation rate coefficient is equal to $-\lambda_1$, where λ_1 is the eigenvalue of $\mathbf{M}$ with the smallest magnitude (all of the eigenvalues are negative). The process of determining the eigenvalues of $\mathbf{M}$ is facilitated by symmetrizing $\mathbf{M}$, i.e., by converting eq 6 to the equation

$$\frac{\mathrm{d}|\mathbf{y}\rangle}{\mathrm{d}t} = \mathbf{G}|\mathbf{y}\rangle \quad (7)$$

where $|\mathbf{y}\rangle$ contains scaled populations and $\mathbf{G}$ is real and symmetric. Because this master equation is irreversible, we obtain directly only the dissociation rate coefficient. However, the reverse association rate coefficient can be obtained from detailed balance. The validity of this approach has been demonstrated by Miller and Klippenstein.[27] In the present work we use both the two-dimensional ME described above and a one-dimensional ME in which E, the total vibrational−rotational energy of the molecule, is the independent variable.

In the ME calculations, experimental values[28] are used for the zero-point inclusive dissociation energy (36 168 cm^{-1}), frequencies (3019, 2917, 1543, and 1306 cm^{-1}), and rotational constant (5.24 cm^{-1}) of CH_4 and for the frequencies (3161, 3004,

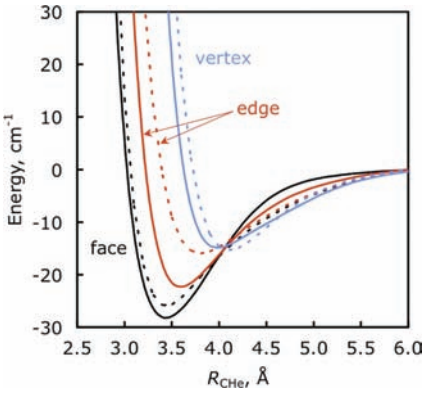

Figure 1. CH_4 + He interaction energy as a function of the C−He distance for three approaches calculated using the MP2/aug′-cc-pVDZ (dashed) and QCISD(T)/CBS (solid) methods.

1396, and 606 cm^{-1}) and rotational constants (9.58 and 4.74 cm^{-1}) of CH_3. Lennard-Jones parameters[29] are used to compute the CH_4 + He collision frequency $Z = Z_{LJ}$, where $\sigma_{LJ} = 2.94$ Å (the arithmetic mean of 2.55 and 3.33 Å, the collision radii of He and CH_4, respectively), and $\epsilon_{LJ} = 25.8$ cm^{-1} (the geometric mean of 7.0 and 94.9 cm^{-1}, the Lennard-Jones well depths for He and CH_4, respectively). The CH_3 + H capture rate coefficient is taken from the direct VRC-TST calculations of ref 30. Master equation calculations were carried out using Variflex.[31]

B. Direct Classical Trajectories. ***Potential Energy Surface.*** The CH_4 + He system has a weak van der Waals well (∼28 cm^{-1}) that may play a role in controlling energy transfer at low temperatures. Previous trajectories studies[14] have indicated that calculated energy transfer averages may be sensitive to the "softness" of the intermolecular repulsive wall. Here we use fully dimensional, fully anharmonic direct dynamics to describe the joint intermolecular *and* intramolecular potential energy surface.

Several levels of quantum chemistry suitable for direct dynamics calculations (MP2 and DFT, with small to moderately sized basis sets) were validated against QCISD(T)/CBS calculations, where the complete basis set (CBS) limit[32] was estimated from aug-cc-pVDZ and aug-cc-pVTZ calculations. In general, DFT methods do not properly describe dispersion interactions, and this was confirmed by our tests of several widely used functionals and basis sets. (Note that we did not test DFT methods designed specifically for nonbonding interactions. Several such functionals are actively being developed.[33]) MP2 results were found to be very sensitive to the size of the basis set and most likely suffer from basis set superposition error. A good compromise of accuracy and computational efficiency was obtained using the restricted MP2 method with the aug′-cc-pVDZ basis set.[34] The "aug′-" prefix denotes that the aug-cc-pVDZ basis set[35] is used for the "heavy" atoms (C and He), and the cc-pVDZ basis set[36] is used for H.

Potential energy curves for three approaches of the He atom to CH_4 are shown in Figure 1. In general, the van der Walls interactions and repulsive wall shapes and distances predicted by the MP2/aug′-cc-pVDZ method are in good agreement with the QCISD(T)/CBS calculations. A comparison may also be made with the previous work of Calderoni et al.,[37] who characterized the potential energy surface for this system at several levels of theory. The highest level of theory presented in ref 37 (MP4/aug-cc-pVTZ augmented with additional bond functions) predicts well depths of 28.1, 21.5, and 14.4 cm^{-1} for the face, edge, and vertex approaches, respectively. These values are in excellent agreement with the QCISD(T)/CBS calculations reported here (28.1, 22.3, and 14.8 cm^{-1}). Similar good agreement is obtained for the calculated MP4/aug-cc-pVTZ and QCISD(T)/CBS equilibrium and repulsive wall distances.

The MP2/aug′-cc-pVDZ method predicts CH_4 frequencies of 3207, 3063, 1551, and 1323 cm^{-1} and a rotational constant of 5.19 cm^{-1} in good agreement with the experimental values. The calculated $CH_4 \rightarrow CH_3$ + H classical dissociation energy is 37 252 cm^{-1}.

The restricted MP2 method used in the direct trajectory calculations is not appropriate for extended C−H distances. The maximum C−H distance accessed during the trajectory simulations is 1.8 Å, however, which is less than the distance at which the restricted and unrestricted MP2 solutions begin to diverge (∼2.2 Å).

It is unclear how sensitive the predicted energy transfer parameters are to details of the potential energy surface (e.g., vibrational frequencies, van der Waals well depths, etc). The restricted MP2/aug′-cc-pVDZ method provides reasonable accuracy, while retaining the computational efficiency to allow for the computation of thousands of direct dynamics CH_4 + He trajectories.

The Gaussian03[38] and Molpro 2006[39] program packages were used.

Initial Conditions. Due to the relatively high computational cost associated with direct trajectories, initial conditions were prepared such that sampling over the phase space of CH_4, the thermal distribution of the relative collision energy, and the impact parameter were carried out simultaneously. This approach allows for the calculation of the average overall and downward energy transfer with good precision without resolving the more complicated underlying dependence of these averages on the various collision parameters. The sensitivity of the computed energy transfer moments on the initial rotational state of CH_4 was considered explicitly.

Ensembles of CH_4 + He collisions with fixed values of J' (the initial angular momentum of CH_4) and T_{bath} (the temperature of the bath gas) were generated as follows. The initial coordinates and momenta for CH_4 were sampled evenly in time from several equilibration trajectories of isolated CH_4. The equilibration trajectories were run for 1000 fs with a fixed time step of 0.25 fs and were initiated from the minimum-energy structure of CH_4 with zero total angular momentum, a total energy equal to 95% of the rotationless MP2/aug′-cc-pVDZ $CH_4 \rightarrow CH_3$ + H bond dissociation energy, and randomly assigned momenta. The initial vibrational energy of CH_4 was scaled to $E'_{vib}(J')$, which depends on J' as discussed below, and the corresponding rotational energy $E'_{rot}(J')$ was added about a random axis. (Note that the nuclear coordinates were not adjusted when the vibrational energy was scaled. The energy adjustments were small, and dynamical differences between our ensemble and a true microcanonical ensemble at E'_{vib} are likely negligible.)

We wish to study energy transfer in deactivating collisions near the dissociation threshold. The vibrational energy required for rotationally adiabatic dissociation E_{diss} decreases as a function of rotational excitation due to the geometry dependence of the rotational energy. In Figure 2, the MP2/aug′-cc-pVDZ rotationally adiabatic vibrational dissociation energies for CH_3 + H are shown as a function of J and its projection K. (The rotational symmetry of the system is that of a symmetric top along the minimum energy path for dissociation.) We set $E'_{vib}(J') = 0.95$ $[E_{diss}(J', K' = 0) + E_{diss}(J', K' = J')]$, which decreases with increasing J'. The initial total energy for CH_4 was therefore E'

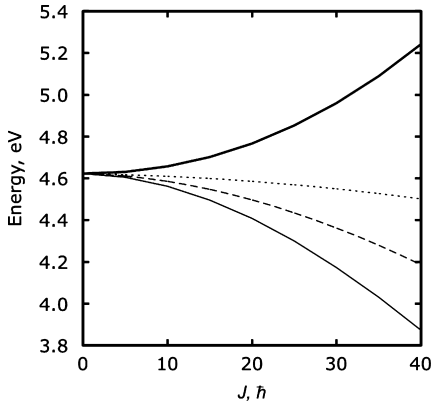

Figure 2. Vibrational dissociation energy (E_{diss}) for CH_4 as a function of rotational excitation J for $K = 0$ (thin solid) and $K = J$ (thin dotted). The average of these curves (thin dashed) is used to define the initial vibrational energy in the trajectory calculations. The sum of the average vibrational energy and the rotational energy (i.e., the total energy of CH_4) is also shown (heavy solid).

$= E'_{vib} + E'_{rot}$, which increases with J'. This strategy differs from previous studies of the effect of rotational excitation on energy transfer, where typically as the initial rotational energy was varied, either the initial vibrational energy or the total energy was held fixed. Here, the initial vibrational energy was set as a fixed fraction of the dissociation energy, which varies with J'.

Several studies have indicated that energy transfer depends linearly on E'. Lendvay and Schatz,[12] however, reported that energy dependence is minor at sufficiently low or high E'. Unfortunately, we cannot readily perform extensive energy dependence tests here, and our choice of E'_{vib} is one source of uncertainty in the present study.

The square of the impact parameter b was sampled evenly from 0 to b^2_{max}, the CH_4 fragment was given a random orientation, and its center of mass was placed at a distance R' from He. The initial relative collision energy E'_{trans} was sampled from a Maxwell distribution for each temperature T_{bath}. The CH_4 + He collisions were integrated using the Bulirch−Stoer variable step size integrator[40] and an integrator tolerance small enough to ensure total energy and total angular momentum conservation of at least 10 cm^{-1} and 10^{-3} ħ per trajectory. Average total energy and total angular momentum conservation were 2 cm^{-1} and 2×10^{-4} ħ per trajectory. Trajectories were terminated when He was at least a distance of R from the center of mass of CH_4. Fragmentation of CH_4 was not energetically allowed. Each simulation consisted of $N_{traj} = 200-475$ trajectories. Checks were made to ensure that the results of the simulation did not depend on our choice of b_{max} (4.25 Å), R' (6 Å), or R (5.5 Å). Along with the rule for E'_{vib}, the parameters defining each energy transfer simulation are J' and T_{bath}.

Final State Analysis. If the final CH_4 + He separation is chosen to be suitably large, the final relative translational energy E_{trans} and total angular momentum of CH_4, J, can be calculated unambiguously. By conservation of energy, the change in the total energy of CH_4 for trajectory i is $\Delta E_i = E_{trans,i} - E'_{trans,i}$. The following energy transfer averages were calculated for each ensemble

$$\langle \Delta E \rangle = \frac{Z_{HS}}{Z_{LJ}} \sum_{i=1}^{N_{traj}} \Delta E_i / N_{traj} \tag{8}$$

$$\langle \Delta E^2 \rangle^{1/2} = \sqrt{\frac{Z_{HS}}{Z_{LJ}} \sum_{i=1}^{N_{traj}} \Delta E_i^2 / N_{traj}} \tag{9}$$

$$\langle \Delta E_d \rangle = -\frac{Z_{HS}}{Z_{LJ}} \sum_{i=1}^{N_{traj}} \min(\Delta E_i, 0) / N_d \tag{10}$$

where Z_{HS} is the hard sphere collision frequency

$$Z_{HS} = \pi b^2_{max} \sqrt{8 k_B T_{bath} / \pi \mu} \tag{11}$$

Z_{LJ} is the Lennard-Jones collision frequency

$$Z_{LJ} = \pi \sigma^2_{LJ} \sqrt{8 k_B T_{bath} / \pi \mu} / (0.7 + 0.52 \log_{10}(k_B T_{bath} / \epsilon_{LJ})) \tag{12}$$

N_d is the number of deactivating collisions, μ is the reduced mass of CH_4 and He, and σ_{LJ} and ϵ_{LJ} are Lennard-Jones parameters.

The per-collision energy transfer averages in eqs 8−10 are scaled by Z_{HS}/Z_{LJ}, and a consistent set of Lennard-Jones collision parameters were used when evaluating Z in the ME calculations (i.e., $Z = Z_{LJ}$ in eq 1). In the trajectory simulation, the collision frequency depends on b_{max} and is given by Z_{HS}. The chemically important quantity is the energy transferred per unit time (which is the product of the collision frequency and the average energy transferred per collision), and the scaling in eqs 8−10 ensures that this quantity is treated equally in the ME and trajectory calculations, despite the differing collision frequencies. In general, calculated or measured per-collision energy transfer moments will depend on the choice of collision frequency, and scaling is required to make meaningful comparisons if different collision frequencies are used.[5]

One may define an effective hard sphere collision diameter based on the Lennard-Jones potential by equating eqs 11 and 12 and solving for b_{max}. This value will be denoted as b_{LJ} and depends on temperature.

The change in the rotational energy is defined as

$$\Delta E_{rot,i} = \frac{J_i(J_i+1)\hbar^2}{2I_{eq}} - \frac{J'_i(J'_i+1)\hbar^2}{2I_{eq}} \tag{13}$$

where I_{eq} is the MP2/aug′-cc-pVDZ moment of inertia for the equilibrium configuration of CH_4. The change in the vibrational energy is calculated $\Delta E_{vib,i} = \Delta E_i - \Delta E_{rot,i}$.

One-sigma uncertainties are reported for the average energy transfer parameters, as estimated using the bootstrap resampling method.[13,41,42] This approach provides uncertainty estimates for unbiased samples without prior knowledge of the underlying distribution function. Tests were carried out to show that the predicted uncertainties decreased roughly as the inverse of the square root of the number of trajectories.

III. Results and Discussion

A. Energy Transfer. Energy transfer simulations were carried out for $T_{bath} = 300$, 600, 1150, and 2000 K and for several values of J', as summarized in Table 1. Bootstrap uncertainty estimates indicate that $\langle \Delta E_d \rangle$ and $\langle \Delta E^2 \rangle^{1/2}$ are converged to 10−20% despite the relatively modest number of trajectories in each simulation (200−475).

In Figure 3, $-\langle \Delta E \rangle$, $-\langle \Delta E_{rot} \rangle$, and $-\langle \Delta E_{vib} \rangle$ are plotted as a function of J'. We note that in thermal rotational distributions of CH_4, the average values of J at 300, 600, 1150, and 2000 K are 5.1, 7.4, 10.5, and 14.0 ħ, respectively. In the limit where rotational energy is uncoupled from vibrational energy, rotational energy transfer may be expected to be positive for rotational quantum numbers less than the thermal averages (as the bath heats up the system rotationally) and negative for higher rotational quantum numbers (as the bath cools down the system

TABLE 1: Calculated Energy Transfer Averages (cm^{-1})

T_{bath}, K	J, $\hbar$	E'_{vib}, eV	E'_{rot}, eV	E', eV	N_{traj}	$\langle\Delta E_d\rangle$	$-\langle\Delta E\rangle$	$\langle\Delta E^2\rangle^{1/2}$
300	0	4.39	0.00	4.39	245	75 ± 10	−31 ± 12	126 ± 14
	10	4.36	0.07	4.43	210	188 ± 25	54 ± 21	198 ± 20
	20	4.27	0.27	4.54	210	282 ± 48	109 ± 30	285 ± 39
600	0	4.39	0.00	4.39	220	77 ± 13	−167 ± 31	287 ± 41
	10	4.36	0.07	4.43	200	203 ± 29	5 ± 29	245 ± 27
	20	4.27	0.27	4.54	200	337 ± 49	91 ± 36	303 ± 32
1150	0	4.39	0.00	4.39	215	94 ± 15	−290 ± 53	465 ± 90
	10	4.36	0.07	4.43	250	294 ± 38	−90 ± 44	399 ± 25
	20	4.27	0.27	4.54	335	628 ± 89	164 ± 62	653 ± 79
	30	4.14	0.60	4.74	340	654 ± 93	264 ± 68	726 ± 94
2000	0	4.39	0.00	4.39	285	138 ± 28	−451 ± 65	641 ± 90
	20	4.27	0.27	4.54	375	740 ± 99	−26 ± 81	856 ± 73
	40	3.98	1.06	5.03	475	1101 ± 188	343 ± 124	1443 ± 321

rotationally). The present results show positive rotational energy transfer for low J' and negative rotational energy transfer for larger J', in agreement with this general trend. The value of J' at which the average rotational energy transferred is zero, however, is shifted to larger values of J' (by a factor of ∼1.5) than would be expected based on the limit uncoupled rotational motion discussed above. This shift can be attributed qualitatively to the coupling of the rotational and vibrational manifolds, where the near-threshold vibrational energies likely heat the system rotationally, shifting the rotational energy transfer curves in Figure 3 downward.

Average vibrational energy transfer is found to be generally smaller in magnitude than and inversely related to average rotational energy transfer. The averages in Figure 3 obscure the significance of rotational−vibrational energy transfer, and it is difficult to make meaningful interpretations of the mechanism of energy transfer based on these averages alone. Rotational−vibrational energy transfer correlation coefficients[5] computed for each of the ensembles were found to vary from −0.5 to −0.7. These values support the inverse rotational−vibrational energy transfer correlation suggested in Figure 3. No clear trends in the correlation coefficients emerged with respect to J' or T_{bath}. Overall, these considerations suggest that both rotational−vibrational energy transfer and energy transfer from the bath gas play a role in determining the overall energy transfer.

In Figure 4, average downward energy transfer is shown as a function of impact parameter for the (T_{bath}/K, $J'/\hbar$) = (300, 10), (600, 10), (1150, 10), and (2000, 20) simulations. Trajectories were binned as a function of b^2 with a bin size of 2 Å^2, such that each bin contains approximately equal numbers (N_{traj}/9) of trajectories. The noise in the plots is due to the relatively poor statistics for each bin. Figure 4 indicates that the present calculations are likely converged with respect to b_{max} (4.25 Å) for our quoted uncertainty (10−20%). We note that the effective hard sphere diameters based on the Lennard-Jones potential b_{LJ} are 2.7−2.3 Å for 300−2000 K and are significantly shorter than the range over which significant energy transfer occurs.

We find that $\langle\Delta E^2\rangle^{1/2}$ also increases with respect to the temperature of the bath gas and, typically, with J'. Troe showed[43] that if one assumes an exponential down model, the moments $\langle\Delta E\rangle$, $\langle\Delta E_d\rangle$, $\langle\Delta E_u\rangle$, and $\langle\Delta E^2\rangle^{1/2}$ are related by

$$\langle\Delta E\rangle = \langle\Delta E_u\rangle - \langle\Delta E_d\rangle \tag{14}$$

where $\langle\Delta E_u\rangle$ is the average upward energy transfer and

$$\langle\Delta E^2\rangle^{1/2} = \sqrt{2\frac{\langle\Delta E_u\rangle^3 + \langle\Delta E_d\rangle^3}{\langle\Delta E_u\rangle + \langle\Delta E_d\rangle}} \tag{15}$$

We used the present calculated values of $\langle\Delta E_d\rangle$ and $\langle\Delta E_u\rangle$ to test whether our energy transfer moments satisfied eqs 14 and 15. The values of $\langle\Delta E\rangle$ estimated using eq 14 show qualitatively correct trends with respect to J' and T_{bath} but deviate from the directly calculated values (given in Table 1) by more than the combined statistical uncertainty. Using eq 15 to estimate $\langle\Delta E^2\rangle^{1/2}$ results in values that deviate from the calculated values by 5−50% and that are typically too high. Equations 14 and 15 are not satisfied due to the "long tail" of the true nonexponential probability distribution of ΔE, as discussed next.

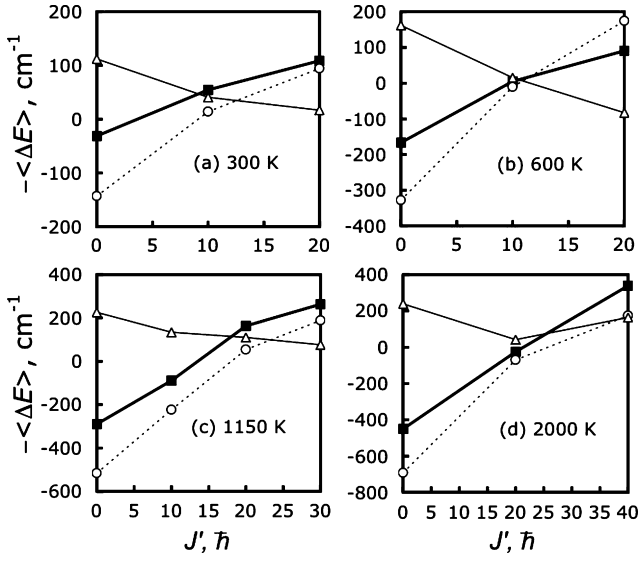

Figure 3. Average total (squares), rotational (circles), and vibrational (triangles) energy transfer.

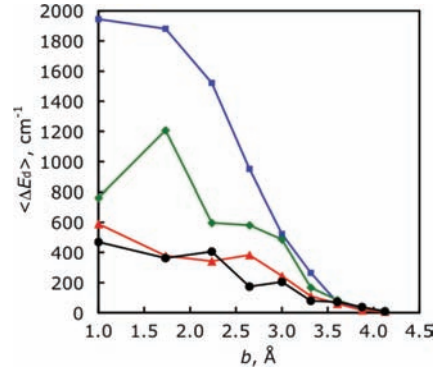

Figure 4. Average downward energy transfer as a function of impact parameter for $J' = 10\ \hbar$ and $T_{bath} = 300$ (circles), 600 (triangles), and 1150 K (diamonds) and for $J' = 20\ \hbar$ and $T_{bath} = 2000$ K (squares).

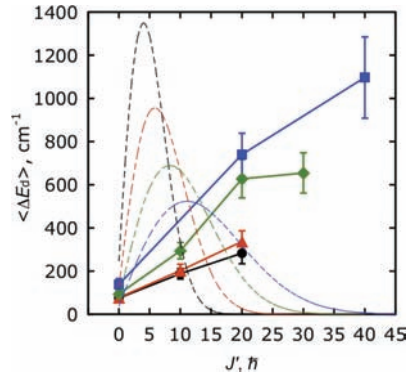

Figure 5. Average downward energy transfer as a function of J' for $T_{bath} = 300$ (circles), 600 (triangles), 1150 (diamonds), and 2000 K (squares). Thermal probability distributions of J' for the same temperatures with arbitrary scaling are shown as dashed lines.

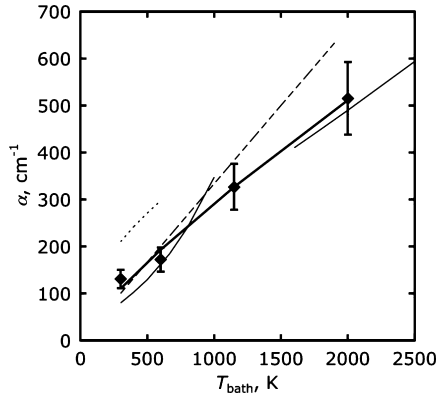

Figure 6. Calculated energy transfer parameters as a function of T_{bath} (diamonds), along with a best fit of these data to eq 9 (thick solid line). The previous fitted values of Miller et al.[21] (300−1000, 1600−2500 K; thin solid lines), Golden[22] (300−2000 K; thin dashed line), and Seakins et al.[20] (300−600 K; thin dotted line) are also shown.

Although the relatively small number of trajectories prevents a quantitative investigation, our results are consistent with a biexponential probability distribution of ΔE. We find that 3−6% of trajectories in each ensemble have $\Delta E_d > 5\langle\Delta E_d\rangle$, and these trajectories may be identified as supercollisions. (In an exponential distribution, less than 1% of trajectories would satisfy this requirement.) Supercolllisions contribute significantly to the energy transfer averages. Arbitrarily removing supercollisions lowers the calculated values of $\langle\Delta E_d\rangle$ by 15−40%. This is potentially a cause for concern in the present study, as here we are limited in the number of trajectories we can compute, and our results may not be converged with respect to the long tail of the biexponential distribution. Clearly, supercollisions making up only a few percent of collisions suggests that the lower limit on the number of trajectories required to obtain meaningful energy transfer averages is at least a few hundred and is close to the number of trajectories carried out in the present study.

The average downward energy transfer $\langle\Delta E_d\rangle$ for each simulation is plotted in Figure 5. The results suggest a near linear dependence on J', with a slope and an intercept that both increase with the temperature of the bath gas.

As discussed in section II.A, in our implementation of the ME, α in eq 5 is identified with a temperature dependent value of $\langle\Delta E_d\rangle$ that is independent of J'. To obtain α from the present set of calculated values of $\langle\Delta E_d\rangle$, some averaging over J' is required. It is not clear which average over J' is the most appropriate for use in ME calculations. We test the simple approach of averaging a linear least-squares fit to the data in Figure 5 for each T_{bath} over a thermal distribution of J'. The thermal distributions of J' are shown in Figure 5, and the resulting values of α are shown in Figure 6.

The calculated values of α increase with temperature, as expected from numerous previous studies of energy transfer. As seen in Figure 5, we may identify two sources for this temperature dependence. First, for a given value of J', $\langle\Delta E_d\rangle$ increases with temperature. Second, the thermal distribution of J' is shifted to higher values at higher temperatures, and these higher values of J' are also associated with higher values of $\langle\Delta E_d\rangle$. The identification of these two effects may aid in developing simple models of energy transfer.

The four calculated values of α for $T = 300-2000$ K were fit to a two-parameter model

$$\alpha = \alpha_{300}(T/300\text{K})^n \quad (16)$$

with $n = 0.81$ and $\alpha_{300} = 110$ cm^{-1} by minimizing the rms error. We note that linear or near-linear dependence on temperature has been reported for several systems, and our results are fit reasonably well (although less well) by $n = 0.90$ and $\alpha_{300} = 95$ cm^{-1} or $n = 1.0$ and $\alpha_{300} = 80$ cm^{-1}.

Assuming a linear temperature dependence for α ($n = 1$), Golden[22] recently fit the results of ME calculations to experimental association[23] and dissociation[24] rates in He to obtain $\alpha_{300} = 100$ cm^{-1}. The values derived in that study are shown in Figure 6 and are in good agreement with the calculated ones presented here.

Seakins et al.[20] studied the association kinetics of deuterium-substituted methyl radicals with deuterium atoms experimentally. They used their measured rate coefficients to obtain a high-pressure limit for the unsubstituted $CH_3 + H$ association rate coefficient of 2.9×10^{-10} cm^{-1}, which is in excellent agreement with the direct VRC-TST calculation.[30] They then used this value in ME calculations to show that the 300−500 K experimental data of Brouard et al.[23] are reproduced well using $\alpha_{300} = 210$ cm^{-1} and $n = 0.5$. These values of α are ~1.7 times larger than the present calculated values for this temperature range.

We note that the ME formalisms used by Golden[22] and Seakins et al.[20] differ in several important ways from one another and from the present formalism, and these differences preclude a quantitative comparison of the various estimates of α.

For methane dissociation in Ar, Miller et al.[21] fit the results of a two-dimensional ME calculation to the low-pressure limit measured by Kiefer and Kumaran[44] for 1600−5000 K and to the recommendation of Baulch et al.[25] for 300−1000 K. Their results are shown in Figure 6. The derived values for 1600−2000 K are only 4% lower than the present results for He. At lower temperatures (300−1000 K), there is additional uncertainty in the experimental low-pressure limit, and Miller et al. report fitted values of α that differ by up to 25% from the present results for He.

The present results are in excellent agreement with Hu and Hase's calculated values[7] at 1000 K in Ar (~300 cm^{-1}), which were obtained via trajectory simulations using several empirical potentials.

B. Master Equation Calculations. One- and two-dimensional master equation calculations for $CH_3 + H \rightleftarrows CH_4$ in He were carried out using the calculated values of α. In Figure 7, the predicted association rate coefficients are compared with the experimental measurements of Pilling and co-workers[23] and the recent recommendations of Baulch et al.[25] at 300 and 600 K.

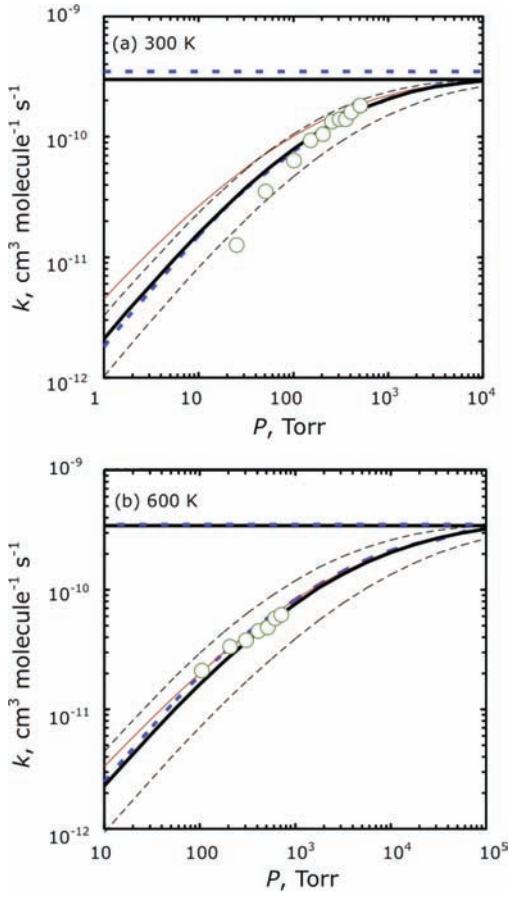

Figure 7. Calculated $CH_3 + H \rightarrow CH_4$ rate coefficient in He at (a) 300 and (b) 600 K using the two-dimensional ME (thick solid line) and the one-dimensional ME (thin solid line). The effect of changing the computed α by a factor of 2 on the two-dimensional rate coefficient is shown by the thin dashed lines. The recommendation of Baulch et al.[25] (thick dotted lines) and the experimental results of Brouard et al.[23] (circles) are also shown. Horizontal lines indicate the high-pressure limit.

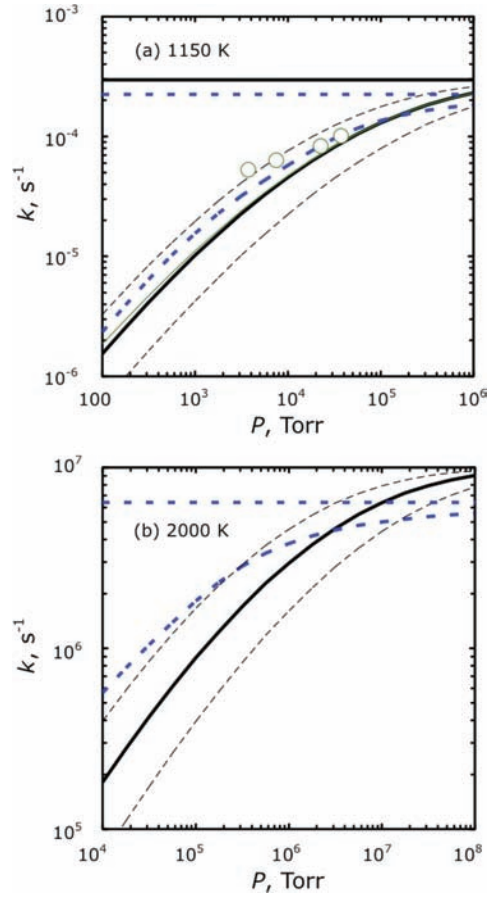

Figure 8. Calculated $CH_4 \rightarrow CH_3 + H$ rate coefficient in He at (a) 1150 and (b) 2000 K using the two-dimensional ME (thick solid line) and the one-dimensional ME (thin solid line). The effect of changing the computed α by a factor of 2 on the two-dimensional rate coefficient is shown by the thin dashed lines. The recommendation of Baulch et al.[25] (thick dotted lines) and the experimental results of Barnes et al.[24] (circles) are also shown. Horizontal lines indicate the high-pressure limit.

At room temperature, the two-dimensional rate coefficient is in excellent agreement with the recent recommendation and is in good agreement with the measured results at pressures greater than ~100 torr. Neither the present results nor the recommended values of Baulch et al. agree with the lowest-pressure experimental measurements; the experimental results suggest a more significant pressure dependence. The one-dimensional rate coefficient overestimates the recommended result for moderate and low pressures. Using the one-dimensional ME formulation, a value of $\alpha = 100\ cm^{-1}$ (25% lower than the calculated value) results in good agreement with the recommended values.

At 600 K, the differences between the one-dimensional and two-dimensional treatments are minor, and the ME results with the calculated value of α are in excellent agreement with the recommended and experimental values.

The sensitivity of the results of the ME calculations to the value of α is also shown in Figure 7. The calculated values of α are clearly more accurate than the results of ME calculations using 2α or α/2. We also tested treating the umbrella motion of CH_3 as an anharmonic oscillator when calculating the association kinetics, and the results were found to be very similar to a full harmonic treatment, differing by less than 15%.

Next we consider the dissociation of CH_4 at 1150 and 2000 K, and the results are shown in Figure 8. At 1150 K, the present dissociation rates are in good agreement with the recommendation of Baulch et al.[25] and with the experimental results of Barnes et al.[24] at high pressures. The lower-pressure experimental values are larger than the rate coefficient predicted here. At 2000 K, the recommendation of Baulch et al. differs significantly from the present rates.

Overall, although experimental rates for $CH_3 + H \rightleftarrows CH_4$ in He are somewhat limited, the values of α obtained from the direct trajectory studies, combined with a single-exponential-down model for energy transfer and a two-dimensional master equation treatment, provide an accurate description of the kinetics of this system.

IV. Conclusions

Direct classical trajectory simulations were used to compute energy transfer parameters for the $CH_3 + H \rightleftarrows CH_4$ reaction in helium. Energy transfer was found to increase with both the initial rotational state of CH_4 and with the temperature of the bath gas. Temperature-dependent energy transfer parameters suitable for use in master equation calculations employing the exponential-down model were obtained by averaging over thermal distributions of the initial rotational state of CH_4. The resulting association and dissociation rate coefficients were found to be in excellent agreement with available experimental results and recent recommendations.

This study demonstrates that trajectory calculations, along with ab initio determinations of energetics and kinetics, can provide a complete first-principles characterization of association and dissociation kinetics.

Acknowledgment. This work is supported by the Division of Chemical Sciences, Geosciences, and Biosciences, Office of Basic Energy Sciences, U.S. Department of Energy. Sandia is a multiprogram laboratory operated by Sandia Corporation, a Lockheed Martin Company, for the United States Department of Energy under Contract No. DE-AC04-94-AL85000.

References and Notes

(1) Barker, J. R.; Golden, D. M. *Chem. Rev.* **2003**, *103*, 4577.
(2) Pilling, M. J.; Robertson, S. H. *Annu. Rev. Phys. Chem.* **2003**, *54*, 245.
(3) Miller, J. A.; Klippenstein, S. J. *J. Phys. Chem. A* **2006**, *110*, 10528.
(4) Stace, A. J.; Murrell, J. N. *J. Chem. Phys.* **1978**, *68*, 3028.
(5) Brown, N. J.; Miller, J. A. *J. Chem. Phys.* **1984**, *80*, 5568.
(6) Gelb, A. *J. Phys. Chem.* **1985**, *89*, 4189.
(7) Hu, X.; Hase, W. L. *J. Phys. Chem.* **1988**, *92*, 4040.
(8) Bruehl, M.; Schatz, G. C. *J. Phys. Chem.* **1988**, *92*, 7223.
(9) Lim, K. F.; Gilbert, R. G. *J. Phys. Chem.* **1990**, *94*, 72; **1990**, *94*, 77.
(10) Lendvay, G.; Schatz, G. C. *J. Phys. Chem.* **1990**, *94*, 8864; **1991**, *95*, 8748; **1992**, *96*, 3752.
(11) Clarke, D. L.; Gilbert, R. G. *J. Phys. Chem.* **1992**, *96*, 8450.
(12) Lendvay, G.; Schatz, G. C. *J. Chem. Phys.* **1993**, *98*, 1034.
(13) Lim, K. F. *J. Chem. Phys.* **1994**, *100*, 7358.
(14) Lenzer, T.; Luther, K.; Troe, J.; Gilbert, R. G.; Lim, K. F. *J. Chem. Phys.* **1995**, *103*, 626. Lenzer, T.; Luther, K. *J. Chem. Phys.* **1996**, *105*, 10944.
(15) Linhananta, A.; Lim, K. F. *Phys. Chem. Chem. Phys.* **1999**, *1*, 3467; **2000**, *2*, 1358; **2002**, *4*, 577.
(16) Yoder, L. M.; Barker, J. R. *J. Phys. Chem. A* **2000**, *104*, 10184.
(17) Ree, J.; Kim, Y. H.; Shin, H. K. *J. Chem. Phys.* **2002**, *116*, 4858.
(18) Brunsvold, A. L.; Garton, D. J.; Minton, T. K.; Troya, D.; Schatz, G. C. *J. Chem. Phys.* **2004**, *121*, 11702.
(19) Bernshtein, V.; Oref, I. *J. Chem. Phys.* **1998**, *108*, 3543. Bernshtein, V.; Oref, I. *Isr. J. Chem.* **2007**, *47*, 205, and references therein.
(20) Seakins, P. W.; Robertson, S. H.; Pilling, M. J.; Wardlaw, D. M.; Nesbitt, F. L.; Thorn, R. P.; Payne, W. A; Stief, L. J. *J. Phys. Chem. A* **1997**, *101*, 9974.
(21) Miller, J. A.; Klippenstein, S. J.; Raffy, C. *J. Phys. Chem. A* **2002**, *106*, 4904.
(22) Golden, D. M. *Int. J. Chem. Kinet.* **2008**, *40*, 310.
(23) Brouard, M.; Macpherson, M. T.; Pilling, M. J.; Tulloch, J. M.; Williamson, A. P. *Chem. Phys. Lett.* **1985**, *113*, 413. Brouard, M.; Macpherson, M. T.; Pilling, *J. Phys. Chem.* **1989**, *93*, 4047.
(24) Barnes, R. W.; Pratt, G. L.; Wood, S. W. *J. Chem. Soc., Faraday Trans. 2* **1989**, *85*, 229.
(25) Baulch, D. L.; Bowman, C. T.; Cobos, C. J.; Cox, R. A.; Just, Th.; Kerr, J. A.; Pilling, M. J.; Stocker, D.; Troe, J.; Tsang, W.; Walker, R. W.; Warnatz, *J. Phys. Chem. Ref. Data* **2005**, *34*, 757.
(26) Miller, J. A.; Chandler, D. W. *J. Chem. Phys.* **1986**, *85*, 4502.
(27) Miller, J. A.; Klippenstein, S. J. *J. Phys. Chem. A* **2004**, *108*, 8296.
(28) *NIST Chemistry WebBook, NIST Standard Reference Database Number 69*; Linstrom, P. J.; Mallard, W. G., Eds.; National Institute of Standards and Technology: Gaithersburg, MD; p 20899; http://webbook.nist.gov (retrieved December 10, 2008).
(29) Hirschfelder, J. O.; Curtiss, C. F.; Bird, R. B. *Molecular Theory of Gases and Liquids*; John Wiley: New York, 1954; pp 1110, 1212.
(30) Harding, L. B.; Georgievskii, Y.; Klippenstein, S. J. *J. Phys. Chem. A* **2005**, *109*, 4646.
(31) Klippenstein, S. J.; Wagner, A. F.; Dunbar, R. C.; Wardlaw, D. M.; Robertson, S. H.; Miller, J. A. VariFlex, version 1.14m, Argonne National Laboratory, 2006.
(32) Martin, J. M. L.; Uzan, O. *Chem. Phys. Lett.* **1998**, *282*, 16.
(33) See, e.g.: Leverentz, H. R.; Truhlar, D. G. *J. Phys. Chem. A* **2008**, *112*, 6909. Wang, Y.; Paldus, B. *Chem. Phys. Lett.* **2007**, *441*, 187.
(34) DelBene, J. E. *J. Phys. Chem.* **1993**, *97*, 107.
(35) Kendall, R. A.; Dunning, T. H., Jr.; Harrison, R. J. *J. Chem. Phys.* **1992**, *96*, 6796.
(36) Dunning, T. H., Jr. *J. Chem. Phys.* **1989**, *90*, 1007.
(37) Calderoni, G.; Cargnoni, F.; Martinazzo, R.; Raimondi, M. *J. Chem. Phys.* **2004**, *121*, 8261.
(38) Frisch, M. J.; Trucks, G. W.; Schlegel, H. B.; Scuseria, G. E.; Robb, M. A.; Cheeseman, J. R.; Montgomery, J. A., Jr.; Vreven, T.; Kudin, K. N.; Burant, J. C.; Millam, J. M.; Iyengar, S. S.; Tomasi, J.; Barone, V.; Mennucci, B.; Cossi, M.; Scalmani, G.; Rega, N.; Petersson, G. A.; Nakatsuji, H.; Hada, M.; Ehara, M.; Toyota, K.; Fukuda, R.; Hasegawa, J.; Ishida, M.; Nakajima, T.; Honda, Y.; Kitao, O.; Nakai, H.; Klene, M.; Li, X.; Knox, J. E.; Hratchian, H. P.; Cross, J. B.; Bakken, V.; Adamo, C.; Jaramillo, J.; Gomperts, R.; Stratmann, R. E.; Yazyev, O.; Austin, A. J.; Cammi, R.; Pomelli, C.; Ochterski, J. W.; Ayala, P. Y.; Morokuma, K.; Voth, G. A.; Salvador, P.; Dannenberg, J. J.; Zakrzewski, V. G.; Dapprich, S.; Daniels, A. D.; Strain, M. C.; Farkas, O.; Malick, D. K.; Rabuck, A. D.; Raghavachari, K.; Foresman, J. B.; Ortiz, J. V.; Cui, Q.; Baboul, A. G.; Clifford, S.; Cioslowski, J.; Stefanov, B. B.; Liu, G.; Liashenko, A.; Piskorz, P.; Komaromi, I.; Martin, R. L.; Fox, D. J.; Keith, T.; Al-Laham, M. A.; Peng, C. Y.; Nanayakkara, A.; Challacombe, M.; Gill, P. M. W.; Johnson, B.; Chen, W.; Wong, M. W.; Gonzalez, C.; Pople, J. A. *Gaussian 03*, revision C.20; Gaussian, Inc.: Wallingford, CT, 2004.
(39) Werner, H.-J.; Knowles, P. J.; Lindh, R.; Manby, F. R.; Schütz, M.; Celani, P.; Korona, T.; Rauhut, G.; Amos, R. D.; Bernhardsson, A.; Berning, A.; Cooper, D. L.; Deegan, M. J. O.; Dobbyn, A. J.; Eckert, F.; Hampel, C.; Hetzer, G.; Lloyd, A. W.; McNicholas, S. J.; Meyer, W.; Mura, M. E.; Nicklaβ, A.; Palmieri, P.; Pitzer, R.; Schumann, U.; Stoll, H.; Stone A. J.; Tarroni, R.; Thorsteinsson, T. MOLPRO, version 2006,.
(40) Press, W. H.; Teukolsky, S. A.; Vetterling, W. T.; Flannery, B. P. *Numerical Recipes in FORTRAN*, 2nd ed.; Cambridge University Press: Cambridge, 1994; pp 716−725.
(41) Efron, B. *Ann. Stat.* **1979**, *7*, 1.
(42) Nangia, S.; Jasper, A. W.; Miller, T. F.; Truhlar, D. G. *J. Chem. Phys.* **2004**, *120*, 3586.
(43) Troe, J. *J. Chem. Phys.* **1977**, *66*, 4745.
(44) Keifer, J. H.; Kumaran, S. S. *J. Phys. Chem.* **1993**, *97*, 414.

JP900802F